Front pinning in capillary filling of chemically coated channels

F. Diotallevi*
Istituto per le Applicazioni del Calcolo CNR V. Policlinico 137, 00161 Roma, Italy

L. Biferale
Dipartimento di Fisica e INFN, Universita' di Tor Vergata, Via della Ricerca Scientifica 1, 00133 Rome, Italy

S. Chibbaro
Istituto per le Applicazioni del Calcolo CNR V. Policlinico 137, 00161 Roma, Italy
and Dipartimento di Ingegneria Meccanica, Universita' di Tor Vergata, Via della Ricerca Scientifica 1, 00133 Rome, Italy

A. Puglisi
CNISM and Dipartimento di Fisica, Universita' La Sapienza, P.le A. Moro 2, I-00185 Rome, Italy

S. Succi
Istituto per le Applicazioni del Calcolo CNR V. Policlinico 137, 00161 Roma, Italy
(Received 8 May 2008; published 8 September 2008)

The dynamics of capillary filling in the presence of chemically coated heterogeneous boundaries is investigated both theoretically and numerically. In particular, by mapping the equations of front motion onto the dynamics of a dissipative driven oscillator, an analytical criterion for front pinning is derived under the condition of diluteness of the coating spots. The criterion is tested against two-dimensional lattice Boltzmann simulations and found to provide satisfactory agreement as long as the width of the front interface remains much thinner than the typical heterogeneity scale of the chemical coating.

DOI: 10.1103/PhysRevE.78.036305 PACS number(s): 47.55.nb, 68.03.Cd, 47.61.Jd

I. INTRODUCTION

The physics of capillary filling, originated with the pioneering works of Washburn [1] and Lucas [2], has provided a constant source of interesting problems in fluid dynamics [3,4]. Recently, with the burgeoning growth of theoretical, experimental, and numerical works on micro- and nanofluidics, the problem attracted a renewed interest [5–8]. Capillary filling is a typical "contact line" problem, in which the subtle nonhydrodynamic effects taking place at the contact point between the liquid-gas and solid phases allow the interface to move, pulled by capillary forces and contrasted by viscous forces. Usually, only the late asymptotic stage is studied, leading to the well-known Lucas-Washburn law [1], which predicts the following relation for the position $z(t)$ of the moving interface inside the capillary:

$$z^2(t) - z^2(0) = \frac{\gamma H \cos(\theta)}{3\mu} t, \tag{1}$$

where γ is the surface tension between liquid and gas, θ is the *static* contact angle, μ is the liquid dynamic viscosity, H is the channel height, and the factor of 3 depends on the geometry of the channel. Here, we focus on a two-dimensional geometry given by two infinite parallel plates, separated by a distance H [see Fig. 1(a)].

One of the practical problems associated with the Lucas-Washburn law is the monotonically vanishing speed [Eq. (1) implies $\dot{z} \simeq t^{-1/2}$] of the liquid front in the late stage of the process. The inertial effects that characterize the initial stage of the filling process decay exponentially in time, thus leading to a higher sensitivity of the front motion to chemical or geometrical defects deposited along the walls. As a result, the front often pins, since even the smallest hydrophobic spot represents a potential barrier that cannot be overcome by a front moving at a vanishingly small speed [9,10]. In static configurations, heterogenous substrates can also lead to the well-known phenomenon of contact angle hysteresis [11–15].

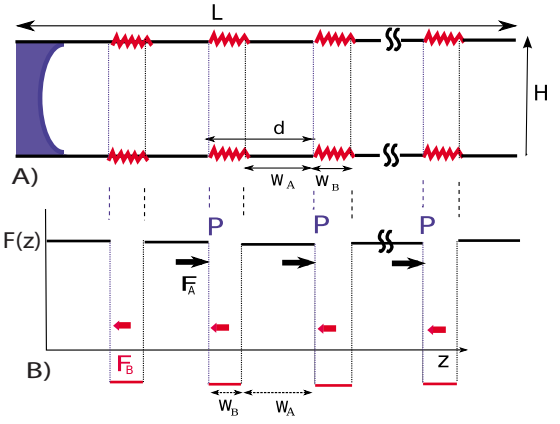

FIG. 1. (Color online) Schematic of the heterogeneous coating. (a) both the walls of the channel are partitioned in an alternate sequence of strips A and B, with different chemical properties (θ_A and θ_B) and different lengths (w_A and w_B). (b) force $f(z)$ as a function of z. In the hydrophilic regions (A) the front is pushed rightwards, while in the hydrophobic ones (B) it is pulled leftwards.

*f.diotallevi@iac.cnr.it

In this work we deal with "chemical" coating, modeled through a position-dependent contact angle $\theta(z)$. In particular, we focus on a dilute regime, where defects (hydrophobic regions) are sparsely deposited on the walls, with a typical interdistance larger than the length scale associated with inertial effects in the flow.

This approach is interesting from the practical standpoint, since in actual experiments, hydrophobic coating is typically used to minimize impurities adsorption at the wall. Thus, it is important to provide a quantitative relation between the average fraction of the hydrophobic surface and the length reachable by the interface along the capillary before pinning occurs. Indeed, this relation would allow a better control of the filling process, determining, for example, the minimal external supply needed to support front propagation up to a given distance.

II. GEOMETRICAL SETUP

We consider a fluid penetrating a channel of length L with periodic hydrophobic spots, as depicted in Fig. 1(a). As we shall see in the following, the periodicity is not an important restriction, as long as the distance between two consecutive hydrophobic spots is large enough—i.e., if the "diluteness" requirement is fulfilled. The channel is coated with an alternate sequence of strips A and B, of length w_A and w_B, respectively, uniformly repeated along the channel length. Regions A and B have different wetting properties, characterized by the contact angles θ_A and θ_B. In the following, we consider the case $\theta_A < \pi/2$ and $\theta_B > \pi/2$, a situation corresponding to a periodic sequence of attracting (hydrophylic) and repelling (hydrophobic) sites [Fig. 1(b)].

In this paper, we investigate the dependence of the front speed on the two lengths w_A and w_B and on the wetting angles θ_A and θ_B. In particular, we show that it is possible to reformulate the filling problem in terms of a damped-forced oscillator, and we develop a procedure that allows for an analytical prediction of the pinning position. This analytical criterion is tested against direct numerical simulations based on the lattice Boltzmann (LB) equation.

III. LUCAS-WASHBURN EQUATION

The Lucas-Washburn equation describing a liquid of density ρ_l and dynamic viscosity μ_l, filling a capillary channel up to a distance z, reads as follows [16–18]:

$$z\frac{d^2z}{dt^2} + \left(\frac{dz}{dt}\right)^2 = -\eta z\frac{dz}{dt} + f(z). \tag{2}$$

The left-hand side (LHS) represents the inertial terms, while the RHS reports the viscous and capillary forces. The parameter $\eta = \frac{12\mu_l}{\rho_l H^2}$ in front of the viscous term defines a characteristic time $t_\eta = \eta^{-1}$, beyond which the dynamics is controlled by the balance between the viscous damping and the capillary force $f(z) = \frac{2\cos[\theta(z)]\gamma}{\rho_l H}$. Here H denotes the height of the channel, supposed for simplicity $2d$.

Equation (2) is exact only in the limit of liquid filling an empty capillary. In the case of a liquid-gas system, the density ratio of the two phases $\alpha = \frac{\rho_g}{\rho_l}$ must be taken into account [16–18].

As we shall see shortly, Eq. (2) stems from the balance between the total momentum change inside the capillary and the force acting on the liquid system. The explicit expression of the viscous drag is obtained assuming a developed Poiseuille profile inside the flow, with speed $u(y) = 6\frac{\bar{u}}{H^2}y(H-y)$. In addition, the front speed is identified with the average flow speed in the channel: namely $\dot{z} \equiv \bar{u} = (1/H)\int_0^H u(y)dy$.

For the case depicted in Fig. 1, the forcing $f(z)$ in the RHS of Eq. (2) is a piecewise constant function, alternating between positive and negative values, as shown in Fig. 1(b). Upon introducing the new variable $q = z^2/2$, Eq. (2) simplifies to

$$\frac{d^2q}{dt^2} = -\eta\frac{dq}{dt} + F(q), \tag{3}$$

where, due to the nonlinear change of coordinates, $F(q)$ is now a *nonperiodic* piecewise constant function of $q(z)$. Note that $F(q)$ has the dimensions of a squared velocity—more precisely, $F(q) = 2V_{cap}V_d\cos[\theta(q)]$, where $V_{cap} = \gamma/\mu_l$ is the capillary speed and $V_d = \nu_l/H$ is the diffusive speed, $\nu_l = \mu_l/\rho_l$ being the kinematic viscosity of the liquid.

Equation (3) describes the motion of a forced damped oscillator with total energy $E(q) = K(q) + V(q)$, where $K(q) = \frac{1}{2}(\frac{dq}{dt})^2$ and $V(q)$, defined by the expression $-\frac{dV}{dq} = F(q)$, are the "kinetic" and "potential" energies, respectively. In the particular case $F(q) = \text{const}$ (homogeneous, noncoated channel), integrating Eq. (3) once, leads to

$$\dot{q}(t) = Ft_\eta + [\dot{q}(t_0) - Ft_\eta]\exp\left(-\frac{(t-t_0)}{t_\eta}\right), \tag{4}$$

which, in the limit $t - t_0 \gg t_\eta$, tends to the asymptotic value

$$\dot{q}(\infty) = v_\infty = Ft_\eta = \frac{\gamma H\cos(\theta)}{6\mu_l}. \tag{5}$$

Taking into account the definition $q = z^2/2$, it is readily checked that Eq. (5) is equivalent to Eq. (1).

IV. CHEMICAL COATING

Let us now focus attention on the case of a dilute dispersion of hydrophobic spots along the channel walls. In other words, we shall always assume that the length of all hydrophilic spots, w_A, is much larger than that of the hydrophobic ones, w_B. Moreover, we also assume the natural condition that the length of hydrophilic spots is large enough to assure that inside each pulling region the front reaches its asymptotic Washburn-Lucas velocity v_∞ given by expression (5). The critical minimal length w_A^{crit} of the hydrophilic region which satisfies the above requirement is easily estimated from Eq. (5). The requirement is that in a time $\Delta t \sim O(t_\eta)$ the front has traveled at least a distance $\Delta q \simeq (w_A^{crit})^2$, leading to

$$w_A^{crit} \sim t_\eta\sqrt{F_A}. \tag{6}$$

Typical values for water-air experiments are $\mu = 10^{-3}$ kg m^{-1} s^{-1}, $\gamma = 72\times10^{-3}$ kg/s^2, yielding a minimum

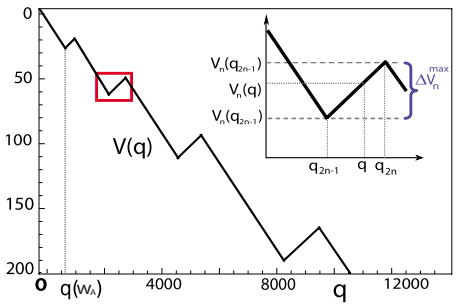

FIG. 2. (Color online) Potential $V(q)$ as a function of q: the ratchet form is clearly visible, as well as the position-increasing potential barriers.

sparseness requirement of the order of $w_A^{crit} \sim 10$ μm for $H = 10$ μm. Of course, if the hydrophilic pulling regions are not long enough, the front dynamics is always in the inertial-transient region of the dynamical evolution of Eq. (3) and the overall dynamics becomes less universal and strongly dependent on the coating details.

V. PINNING CRITERION

Given the definition of $q(z)$, we note that both the potential barrier to be overcome in order to "jump" over the hydrophobic obstacle and the extension of the regions in which the front is accelerated (Fig. 2) are increasing functions of z (and consequently of q). Therefore, if the front manages to approach its asymptotic velocity before encountering the first barrier, it will attain the same asymptotic velocity at the bottom of each of the subsequent potential wells.

This observation opens the way to a simple prediction of the number of barriers the front is able to overcome before being pinned. Given that the kinetic energy $K_\infty^A = \frac{(v_\infty^A)^2}{2}$ accumulated by the particle as it reaches the bottom of the wells remains constant for all n jumps, the final pinning position is fixed by the condition $K_\infty^A < \Delta V_n^{max}$, where ΔV_n^{max} is the ever-increasing heigth of the n potential wells.

Let us focus on the dynamics during the climbing of the nth hydrophobic barrier, located between positions q_{2n-1} and q_{2n} (inset of Fig. 2) and denoted by $\Delta V_n(q) = V(q_{2n}) - V(q)$. While the value of the potential barrier decreases from $\Delta V_n^{max} = V(q_{2n}) - V(q_{2n-1})$ to $\Delta V(q_{2n}) = 0$, kinetic energy is partly converted into potential energy and partly dissipated by viscous forces.

If the coordinate q lies in the range $q_{2n-1} < q < q_{2n}$, the temporal evolution of the potential and kinetic energy obeys the following equations:

$$\frac{d}{dt}\Delta V_n(q) = F_B\sqrt{2K(q)} \tag{7}$$

and

$$\frac{d}{dt}K(q) = -2\eta K(q) + F_B\sqrt{2K(q)}. \tag{8}$$

Equation (8) is obtained from Eq. (3) by multiplying by $\dot{q} = \sqrt{2K(q)}$. Dividing Eq. (7) by Eq. (8) and integrating, we obtain

$$\int_{K_\infty^A}^{K} \frac{dK(q)}{1 - \frac{\sqrt{2K(q)}}{v_\infty^B}} = \int_{\Delta V_n^{max}}^{\Delta V_n} d\Delta V_n(q), \tag{9}$$

where $v_\infty^B = \frac{\gamma H \cos(\theta_B)}{6\mu_l}$. This equation, expressing the kinetic energy K as a function of the potential barrier $\Delta V_n(q)$, is easily solved to yield

$$\Delta V_n - \Delta V_n^{max} \tag{10}$$

$$= v_\infty^B \left[(v_\infty^A - \sqrt{2K}) + v_\infty^B \ln\left(\frac{\sqrt{2K_\infty^A} - v_\infty^B}{\sqrt{2K} - v_\infty^B} \right) \right], \tag{11}$$

where by definition $v_\infty^A = \sqrt{2K_\infty^A}$. The front is pinned whenever two conditions are simultaneously met: kinetic energy is depleted, $K = 0$, and the front position lies inside the hydrophobic region—i.e., $\Delta V_n > 0$.

This yields

$$\Delta V_n = \Delta V_n^{max} + v_\infty^B \left[v_\infty^A + v_\infty^B \ln\left(1 - \frac{\cos(\theta_A)}{\cos(\theta_B)} \right) \right] > 0, \tag{12}$$

where $\Delta V_n^{max} = -F_B(q_{2n} - q_{2n-1})$ is the potential barrier of the nth hydrophobic spot. Expressing ΔV_n^{max} as an explicit function of n one obtains

$$\Delta V_n^{max} = -F_B w_B \left[n(w_A + w_B) - \frac{w_B}{2} \right] \simeq -F_B w_B L_p, \tag{13}$$

where $L_p = n(w_A + w_B) - w_B$ is the pinning length. Inserting Eq. (13) into Eq. (12), after some algebra, the following prediction for the dimensionless pinning length $\tilde{L}_p = L_p/H$ is obtained:

$$\tilde{L}_p \simeq \frac{C_{cap}\cos(\theta_A)}{\tilde{w}_B} \left[1 - \frac{\ln\left(1 + \frac{\cos(\theta_A)}{|\cos(\theta_B)|} \right)}{\frac{\cos(\theta_A)}{|\cos(\theta_B)|}} \right]. \tag{14}$$

Here $C_{cap} = V_{cap}/(72V_d)$ is a constant depending on the capillary parameters, $\tilde{w}_B = w_B/H$ is the dimensionless hydrophobic length, and $-1 < \cos(\theta_B) < 0$. Equation (14) uniquely identifies the pinning region as a function of the coating properties and of the typical extension of the hydrophobic spots, $\tilde{w}_B$. As intuition suggests, the pinning length $\tilde{L}_p$ decreases for intense hydrophobic coating—i.e., for large hydrophobic strength $[\cos(\theta_B) \to -1]$ and for high fraction of geometrical space covered by the hydrophobic component (large $\tilde{w}_B$). Note that Eq. (14) implies that $\tilde{L}_p$ is independent of the length of the hydrophilic regions, $\tilde{w}_A$, while the number of overcome defects, $n \simeq \tilde{L}_p/(\tilde{w}_A + \tilde{w}_B)$, does depend upon it.

Equation (14) highlights two distinguishable limits: that is, *fast-filling* $(\frac{\cos(\theta_A)}{|\cos(\theta_B)|} \gg 0)$ and *slow-filling* $(\frac{\cos(\theta_A)}{|\cos(\theta_B)|} \to 0)$. In the former case Eq. (14) delivers $\tilde{L}_p \simeq C_{cap}\cos(\theta_A)/\tilde{w}_B$, while in the latter the pinning length vanishes like $\tilde{L}_p \simeq C_{cap}\cos(\theta_A)^2/[2\tilde{w}_B|\cos(\theta_B)|]$. These asymptotic expres-

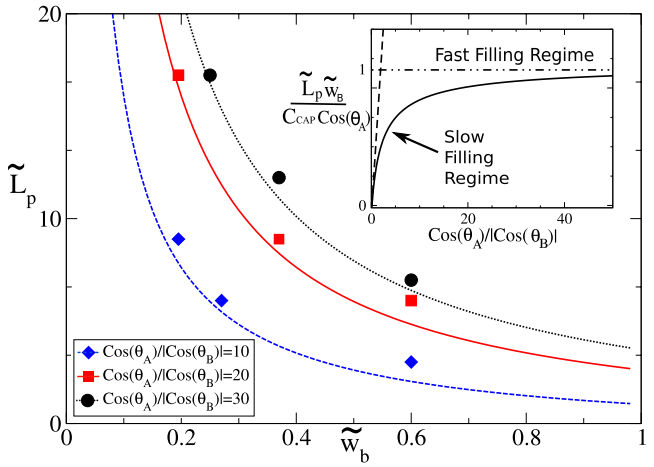

FIG. 3. (Color online) Normalized pinning length $\tilde{L}_p$ as a function of $\tilde{w}_B$ for $|\cos(\theta_A)/\cos(\theta_B)|=10,20,30$. The lines represent the prediction given by Eq. (18), while the symbols are the result of the LB simulations. To match theory and simulation, we have taken $\tilde{w}_B^{eff}=\tilde{w}_B-\tilde{\delta}$ in Eq. (18), where $\tilde{\delta}=\delta/H=0.025$. The other parameters used are $\alpha=0.028$, $\tilde{L}=20$, $\tilde{C}_{cap}=5.7$, and $\theta_B=92$. Inset: normalized pinning length $\tilde{L}_p$ as a function of $|\cos(\theta_A)/\cos(\theta_B)|$. Note the two distinct *fast-filling* and *slow-filling* regimes, as discussed in the text.

sions show that in the fast-filling regime the pinning length $\tilde{L}_p$ grows linearly with the hydrophilic $\cos(\theta_A)$, independently of the hydrophobic strength, and stays finite for any nonzero value of $\tilde{w}_B$. On the other hand, in the slow-filling regime, the pinning length vanishes with the square of the hydrophilic $\cos(\theta_A)$ and is inversely proportional to the hydrophobic one, $\cos(\theta_B)$. Finally, in either case, the pinning length scales inversely with the hydrophobic width $\tilde{w}_B$.

Equation (14) also shows that the quantity $\tilde{L}_p\tilde{w}_B/[C_{cap}\cos(\theta_A)]$ is a universal function of $\cos(\theta_A)/|\cos(\theta_B)|$ (see inset of Fig. 3). Since this function is bounded in the range [0:1], Eq. (14) clearly shows that $\tilde{L}_p$ is always finite, unless $\tilde{w}_B=0$. One may use the previous expression as a first-order guess of the pinning length $\tilde{L}_p$. For a typical case of a capillary filled with water at room temperature, of width $H=10$ μm, and with length of hydrophobic spots of the order of $\tilde{w}_B=0.01-0.1$, we obtain $\tilde{L}_p\simeq 50-500$.

VI. SIMULATIONS

The Lucas-Washburn equation (2) does not take into account two main sources of uncertainity. First, the inlet dynamics may be sensitive to the structure of the reservoir, leading to significant deviations from the Poiseuille profile in the early stage of the filling process. Second, the description does not take into account the dynamical effects induced on the interface by the motion. On the other hand, it is well known that a moving interface may be significantly distorted by the viscous stress induced by the fluid motion, especially close to the contact line. Such a dynamical bending may require the introduction of a *dynamic contact angle* [19–22], leading to a driving force in the Washburn law, which is itself influenced by the interface motion, resulting in an unclosed "bootstrap" problem. Moreover, especially for hydrophilic coating, the shallow fluid wedge at the boundary may induce an extra dissipation [3], which modifies the dissipative terms. Asymptotically, the capillary speed becomes lower and lower, and one may argue that, at large times, the assumptions behind Eq. (2) are increasingly well fulfilled, thereby justifying the neglect of the above-mentioned problems. Still, in many situations the asymptotic "ideal" regime is never reached, and consequentely one needs to assess the influence of the previous effects on the filling process.

To check the validity of the "pinning criterion" on a realistic system, we have resorted to numerical simulations of a two-phase fluid using lattice Boltzmann equations [23–27] in two dimensions to reproduce the capillary filling in presence of coated patterns. The geometry is the same previously discussed (Fig. 1), the only difference being the periodic boundary conditions imposed at the two lateral sides in order to ensure total conservation of mass inside the system. Similar problems, with or without heterogeneous coating, have also been studied recently in [28–31].

The central point of the lattice Boltzmann equation is the time evolution of the kinetic probability density function $f_l(\boldsymbol{x},t)$ [26,27]:

$$f_l(\boldsymbol{x}+\boldsymbol{c}_l\Delta t,t+\Delta t)-f_l(\boldsymbol{x},t)=-\frac{\Delta t}{\tau}[f_l(\boldsymbol{x},t)-f_l^{(eq)}(\rho,\rho\boldsymbol{u})]. \tag{15}$$

Here $\{\boldsymbol{c}_l\}$ is a set of discretized mesoscopic velocities (we adopt the 9 velocities D2Q9 lattice scheme [26,27]), τ is a mean collision time (with Δt a time lapse) which determines the fluid kinematic viscosity ν, and $f_l^{(eq)}(\rho,\rho\boldsymbol{u})$ is the equilibrium distribution, corresponding to the Maxwellian distribution in the continuum limit. From the kinetic distribution, the macroscopic density and momentum fields are defined [26,27]:

$$\rho(\boldsymbol{x})=\sum_l f_l(\boldsymbol{x}),\quad \rho\boldsymbol{u}(\boldsymbol{x})=\sum_l \boldsymbol{c}_l f_l(\boldsymbol{x}), \tag{16}$$

where the sum is intended over all directions pointing out from location $\boldsymbol{x}$. In order to study nonideal effects, the previous description is supplemented with an interparticle forcing F_l, in Eq. (15), which describes the fluid-fluid interactions triggered by inhomogeneities of the density profile, as documented in [24,25,32]. The surface tension γ is determined by tuning the coupling force F_l. Moreover, the introduction of a suitable value for the density ρ_w at the walls [24] allows the definition of a static contact angle θ, which can span the range $\theta\in[0°:180°]$.

To consistently compare the simulation output with the theoretical prediction, we need to take into account the effect of two factors that differentiate simulations from the idealized description given by Eq. (2): (i) the presence of a finite liquid-gas density ratio $\alpha=\rho_g/\rho_l$ and (ii) a finite width δ of the liquid-gas interface in the simulation. In order to take into account the unavoidable "resistance" of the gas occupying the capillary during the liquid invasion, one writes down

the balance between the total momentum change inside the capillary and the force acting on the liquid+gas system. Simple calculations lead to a new equation governing the front dynamics [16,18]:

$$[\alpha L + (1-\alpha)z]\frac{d^2z}{dt^2} + (1-\alpha)\left(\frac{dz}{dt}\right)^2 = -\eta[\alpha L + (1-\alpha)z]\frac{dz}{dt} + f(z). \quad (17)$$

where L is the total length of the channel and $\eta = 12\frac{\nu_l}{H^2(1+6\lambda_l/H)}$, λ_l being the slip length of the fluid. In the limit $\alpha \to 0$ and $\lambda_l \to 0$, one recovers the original equation (2). Equation (17) can be mapped onto the same Eq. (3), only with a slightly different definition of $q=[\alpha L+(1-\alpha)z]^2/2$, and $F(q)=2(1-\alpha)V_{cap}V_d \cos[\theta(z(q))]$.

The pinning criterion, Eq. (14), therefore simply changes to

$$\tilde{L}_p \simeq \frac{\tilde{C}_{cap}\cos(\theta_A)}{\tilde{w}_B}\left[1 - \frac{\ln\left(1+\frac{\cos(\theta_A)}{|\cos(\theta_B)|}\right)}{\frac{\cos(\theta_A)}{|\cos(\theta_B)|}}\right] - \frac{\alpha}{(1-\alpha)}\tilde{L}, \quad (18)$$

where $\tilde{C}_{cap}=C_{cap}(1+6\lambda_l/H)^2/(1-\alpha)$ and $\tilde{L}$ is the dimensionless channel length $\tilde{L}=L/H$. This generalized criterion, denoted from now on as $\tilde{L}_p^{th}$, is tested against LB simulations.

The above equation is exact if evaporation-condensation effects are negligible—i.e., when the gas is pushed out of the capillary—without any interaction with the liquid. This is not the case for most mesoscopic models available in the literature [32,33], which are based on diffusive interface dynamics [34–37]. As shown in a previous paper [16], the dynamics given by (17) is correctly recovered only in the limit of thin interface, $\delta/H \to 0$, and of negligible gas-liquid density ratio, $\alpha \to 0$

For the present case, the existence of a finite interface width δ (generally around five to six grid points) in the simulation has the effect of introducing an effective length of the hydrophobic obstacle, w_B. Therefore, in the following, we compare the simulation results with the solution of Eq. (17) with an effective length of the obstacle, $w_B^{eff}=w_B-\delta$. Besides, in order to recover the correct hydrodynamic limit, the additional requirement $\delta/H \ll 1$ must be fulfilled (Table I).

VII. RESULTS

Figure 3 shows the prediction for the dimensionless pinning length $\tilde{L}_p^{th}$ as a function of the two main parameters $\tilde{w}_B$ and $\cos(\theta_A)/|\cos(\theta_B)|$. The main figure displays three sets of results, corresponding, respectively, to $\cos(\theta_A)/|\cos(\theta_B)| = 10, 20, 30$. The solid lines represent the numerical solutions of Eq. (18), while the symbols correspond to the LB simulation results. As one can see, the numerical results are in satisfactory agreement with the theoretical prediction. It is to be noted that we have limited the numerical comparison up to pinning lengths $\tilde{L}_p^{max} \simeq 15-20$ because of computational constraints.

TABLE I. Comparison between the prediction given by Eq. (18), based on the generalized Washburn equation (17), and the LB simulation, expressed in terms of the number of hydrophobic wells $n_{crit}=[L_p/(w_A+w_B^{eff})-w_B^{eff}]$ that the front manages to overcome. The first column shows the ratio between the interface width δ and channel height H. The simulations were performed taking into account the correction due to the finite width of the interface, $w_B^{eff}=w_B-\delta$. The second column displays the number of wells, n_{crit}^{th}, predicted by Eq. (18), while the third one refers to the LB results n_{crit}^{sim}. Theory and simulations converge towards the same prediction in the limit $\delta/H<0.03$.

δ/H	n_{crit}^{th}	n_{crit}^{sim}	$n_{crit}^{th}/n_{crit}^{sim}$
0.1	2	7	0.28
0.05	5	7	0.71
0.033	8	10	0.83
0.025	12	12	1

In the inset, the universal curve $[1-\ln(1+\frac{\cos(\theta_A)}{|\cos(\theta_B)|})/\frac{\cos(\theta_A)}{|\cos(\theta_B)|}]$ is reported: it is possible to appreciate the two different regimes of *slow filling*, in which the product $\tilde{L}_p\tilde{w}_B/[C_{cap}\cos(\theta_A)]$ grows linearly with $\cos(\theta_A)/|\cos(\theta_B)|$, and *fast filling*, in which this quantity saturates to 1.

It must be noted that the convergence towards $\tilde{L}_p^{th}$ is accomplished only when the width δ of the liquid-gas interface becomes thin enough with respect to the characteristic length H of the system (Table I). In this regime, corresponding to $\delta/H<0.03$, the overall asymptotic trend and the final theoretical pinning position are in agreement with the simulation, as shown in Fig. 4. The discrepancy between the two curves during the initial transient regime is due to the "vena contracta" phenomenon, reflecting the nontrivial matching between the reservoir and the capillary dynamics at the inlet of the simulation setup [38]. Such a small discrepancy can also be reabsorbed into an added mass term in LHS of Eq. (2), as shown quantitatively in [16].

At larger values of the ratio δ/H, the error in $\tilde{L}_p$ becomes higher, and in these cases the simulation systematically gives $\tilde{L}_p > \tilde{L}_p^{th}$ (Table I). Such a discrepancy is connected to the departure from hydrodynamics, for length scales of the order of the interface width, typical of any diffuse-interface description.

The satisfactory agreement between the LB simulations and the hydrodynamical description based on the generalized Washburn equation (17) indicates that effects induced by the distortion of the interface profile are negigible, at least for the choice of coating properties discussed in this work. On the basis of simple hydrodynamical considerations, one would expect that the extra dissipation term induced by the wedge close to the contact line should introduce a correction [19,21,39]:

$$F_{ex} \propto \frac{\dot{z}}{tg(\theta)}\ln(H/\lambda), \quad (19)$$

where λ is the ultraviolet cutoff (inner length scale) up to which hydrodynamics applies. In LB simulations, it is rea-

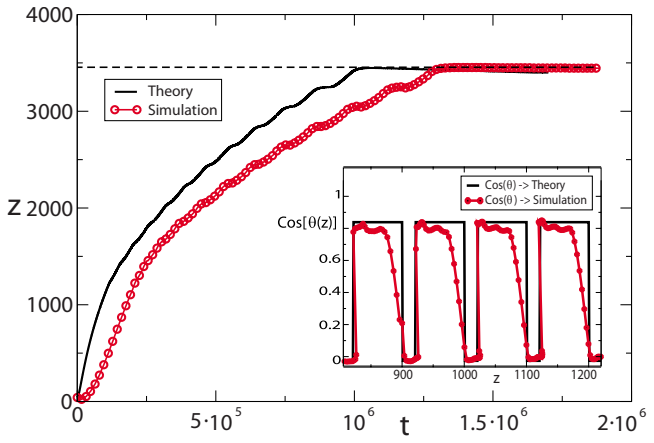

FIG. 4. (Color online) Time evolution of the front coordinate in the LB simulation (symbols) and as numerical solution of Eq. (17) (solid line). The simulation was performed using the following parameters: $\alpha=0.028$, $L=3600$, $H=200$, $w_A=144$, $w_B=56$, $\gamma=0.14$, and $\nu=1/6$. For this case $\delta/H=0.025$, in lattice units. The dashed line marks the prediction of Eq. (18). Inset: comparison between imposed (line) and observed (dots) contact angles: note that while the imposed (static) angle $\cos[\theta(z)]$ is a stepwise function, the dynamic one deviates from it during the hydrophilic-hydrophobic transition. The observed contact angle was obtained by interpolating the front shape with a circle of radius R, so that $\cos(\theta)=H/2R$. Note that, due to the convex shape of the interface, the front coordinate (calculated at $y=H/2$) always precedes the location where the front first meets the hydrophobic region.

sonable to assume $\lambda\sim\delta$. The correction term (19), being localized at the interface, is always subleading at long times, differently from the viscous dissipation that is proportional to the volume occupied by the fluid. This extra stress can change the local interface profile, in particular close to the transition between two regions with different coating properties. This is shown in the inset of Fig. 4, where the effective *dynamic* contact angle is plotted versus the static (microscopic) contact angle imposed by the boundary conditions. As seen, the dynamic profile departs from the static one only when the front enters the hydrophobic region—i.e., where the interface tends to be pinned. Equation (19) suggests that extra dissipation has an effect also for long times in the case of filling with very hydrophilic walls ($\theta_A\sim 0°$) and/or of filling in viscoelastic flows, depending on the rheological properties of the fluid. These interesting issues are left for future research.

VIII. CONCLUSIONS

In conclusion, we have derived an analytical criterion [Eq. (18)] to predict the pinning location of a moving front in a two-dimensional (2D) plane geometry, based on the generalized Lucas-Washburn equation. This criterion has been derived under the assumption of diluteness of hydrophobic spots and has been satisfactorily tested against 2D lattice Boltzmann simulations. We have also discussed limitations of both approaches: the first due to the neglect of interface distortion and extra dissipation at the contact line for Washburn-like equations and the second regarding the effects induced by deviation from hydrodynamics in LB models. We have shown that, in the limit of the fast-filling process ($\theta_A \gg 0$) and for sufficiently thin interfaces, the analytical criterion and the LB simulations are in satisfactory agreement with each other.

Work to extend the pinning criterion to more complex situations, such as in the presence of stochastic heterogeneous coating (not diluted) and/or in the presence of geometrically coated interfaces, is currently underway. Such an investigation is relevant for a direct comparison with experiments, like those reported in [9,10], whose observed stick-slip phenomenon is attributed to the background noise and history of the system.

ACKNOWLEDGMENTS

Financial support through the EC project INFLUS is kindly acknowledged. Valuable discussions with M. Sbragaglia, F. Toschi, and J. Yeomans are kindly acknowledged.

[1] E. W. Washburn, Phys. Rev. **17**, 273 (1921).
[2] R. Lucas, Kolloid-Z. **23**, 15 (1918).
[3] P. G. de Gennes, Rev. Mod. Phys. **57**, 827 (1985).
[4] E. B. Dussan, Annu. Rev. Fluid Mech. **11**, 11 (1979).
[5] L. J. Yang, T. J. Yao, and Y. C. Tai, J. Micromech. Microeng. **14**, 220 (2004).
[6] F. Goldschmidtboeing, M. Rabold, and P. Woias, J. Micromech. Microeng. **16**, 1321 (2006).
[7] U. Thiele and E. Knobloch, New J. Phys. **8**, 313 (2006).
[8] N. R. Tas *et al.*, Appl. Phys. Lett. **85**, 3274 (2004).
[9] E. Schäffer and P. Z. Wong, Phys. Rev. Lett. **80**, 3069 (1998).
[10] E. Schäffer and P. Z. Wong, Phys. Rev. E **61**, 5257 (2000).
[11] M. O. Robbins and J. F. Joanny, Europhys. Lett. **3**, 729 (1987).
[12] H. Kasumaatmaja and J. M. Yeomans, Langmuir **23**, 6019 (2007).
[13] S. Brandon, N. Haimovich, E. Yeger, and A. Marmur, J. Colloid Interface Sci. **263**, 237243 (2003).
[14] S. Brandon and A. Marmur, J. Colloid Interface Sci. **183**, 351355 (1996).
[15] A. Marmur, Colloids Surf., A **116**, 5561 (1996).
[16] F. Diotallevi, L. Biferale, S. Chibbaro, A. Lamura, G. Pontrelli, M. Sbragaglia, S. Succi, and F. Toschi, Eur. Phys. J. B (to be published).
[17] F. Diotallevi, L. Biferale, S. Chibbaro, G. Pontrelli, S. Succi, and F. Toschi, Eur. Phys. J. B (to be pubilshed).
[18] G. Cavaccini, V. Pianese, A. Jannelli, S. Iacono, and R. Fazio, Lect. Ser. Comput. Comput. Sci. **7**, 66 (2006).
[19] J. Eggers, Phys. Rev. Lett. **93**, 094502 (2004).
[20] J. Eggers, Phys. Fluids **16**, 3491 (2004).

[21] R. G. Cox, J. Fluid Mech. **168**, 169 (1986).
[22] C. Huh and L. E. Scriven, J. Colloid Interface Sci. **35**, 85 (1971).
[23] R. Benzi, S. Succi, and M. Vergassola, Phys. Rep. **222**, 145 (1992).
[24] R. Benzi, L. Biferale, M. Sbragaglia, S. Succi, and F. Toschi, Phys. Rev. E **74**, 021509 (2006).
[25] M. Sbragaglia, R. Benzi, L. Biferale, S. Succi, K. Sugiyama, and F. Toschi, Phys. Rev. E **75**, 026702 (2007).
[26] D. Wolf-Gladrow, *Lattice-Gas Cellular Automata And Lattice Boltzmann Models* (Springer, New York, 2000).
[27] S. Succi, *The Lattice Boltzmann Equation* (Oxford Science, Oxford, 2001).
[28] J. Zhang and D. Y. Kwok, Langmuir **22**, 4998 (2006).
[29] M. Latva-Kokko and D. H. Rothman, Phys. Rev. Lett. **98**, 254503 (2007).
[30] X. Jia, J. B. Laughlin, and Kontomaris, Math. Comput. Simul. **72**, 156 (2006).
[31] C. Kunert and J. Harting, Phys. Rev. Lett. **99**, 176001 (2007).
[32] X. Shan and H. Chen, Phys. Rev. E **47**, 1815 (1993).
[33] A. J. Briant, A. J. Wagner, and J. M. Yeomans, Phys. Rev. E **69**, 031602 (2004).
[34] D. Jacqmin, J. Fluid Mech. **402**, 57 (2000).
[35] P. Seppecher, Int. J. Eng. Sci. **34**, 977 (1996).
[36] L. M. Pismen, Phys. Rev. E **64**, 021603 (2001).
[37] L. M. Pismen, Colloids Surf., A **206**, 11 (2002).
[38] J. Szkeley, A. W. Neumann, and Y. K. Chuang, J. Colloid Interface Sci. **69**, 486 (1979).
[39] O. V. Voinov, Fluid Dyn. **11**, 714 (1976).